Research Article

Drug Testing and Analysis

Received: 17 October 2008 Revised: 18 December 2008 Accepted: 18 December 2008 Published online in Wiley Interscience:

(www.drugtestinganalysis.com) DOI 10.1002/dta.17

Computational and vibrational spectroscopic studies of ipratropium bromide

H. R. H. Ali,[1,3] H. G. M. Edwards,[1]* J. Kendrick[2] and I. J. Scowen[1]

In this study, ipratropium bromide is investigated using vibrational spectroscopy and quantum chemical calculations. The structure of ipratropium bromide was optimised using density functional theory calculations and the geometry optimisation has been carried out on two conformations with and without intramolecular hydrogen bonding. Infrared and Raman spectra were calculated from the optimised structures. Many modes in the calculated spectra could be matched with the experimental spectra and a description of the modes is given. By analysis of the theoretical vibrational modes, it is shown that ipratropium bromide specimens are likely to be a mixture of the two conformations with and without intramolecular hydrogen bonding. In addition, several spectral features and band intensities in the CH and OH stretching regions are explained. Quantum mechanical calculations allowed improved understanding of ipratropium bromide and its vibrational spectra.

Keywords: Raman; infrared spectroscopy; ipratropium; respiratory pharmaceuticals; quantum chemical calculations; hydrogen bond

Introduction

Ipratropium bromide (IPRA), chemically known as 8-isopropyl-noratropine-methylbromide, a quaternary ammonium compound with antimuscarinic properties, is used as a bronchodilator for the maintenance and treatment of bronchospasms associated with chronic obstructive pulmonary disease[1] (Scheme 1).

In recent years the evolution of in-process analysis has required the development and application of rapid and reliable nondestructive analytical tools. As spectroscopic techniques offer these possibilities, methods such as near-infrared analysis have become well established within the pharmaceutical industry.[2–5] FT-Raman spectroscopy is also becoming increasingly popular as a technique for the analysis of the solid state of pharmaceutical crystals[6–8] and for offline quantitative analysis.[9–14]

Raman spectroscopy provides information about the structure of a molecule complementary to the data obtained from infrared analysis. Both techniques combined together to provide complete vibrational information about a molecule. However, Raman spectroscopy has some distinct advantages for pharmaceutical analysis in that sample preparation is minimal and often the Raman spectrum of a sample can be recorded inside its packaging (glass vial, plastic container, blister pack) without significant interference.[6,8] Raman spectroscopy also allows analysis in aqueous environments as water is a weak Raman scatterer, whereas water often masks spectral features of interest in an IR spectrum.

In this paper, we present the Raman spectrum of ipratropium bromide for the first time and molecular assignments are proposed on the basis of quantum chemical calculations using BLYP density functional theory with a 6-31G* basis set and vibrational frequencies and intensities predicted within the quasiharmonic approximation. Several spectral features and band intensities in the CH and OH stretching regions and the potential presence of an internal hydrogen bond are thereby explained to provide molecular structural information about IPRA that can be employed to aid in its process monitoring.

Experimental

Materials

Specimens of IPRA were obtained from Sigma Aldrich Chemical Co. and were used without further purification.

Raman spectroscopy

Fourier-transform Raman spectroscopy was carried out using a Bruker IFS 66 instrument with an FRA 106 Raman module attachment and a Nd^{+3}/YAG laser operating at 1064 nm in the near infrared. The powdered specimens were examined in aluminium cups. The spectra were recorded at 4 cm^{-1} spectral resolution and 500 spectral scans accumulated to improve signal-to-noise ratios. Laser powers were maintained at 200 mW at the samples.

Infrared spectroscopy

The IR spectra were recorded as KBr discs (1 : 200) using a Digilab Scimitar Series spectrometer. The spectra were recorded in the range of 650–4000 cm^{-1} at 4 cm^{-1} spectral resolution with the accumulation of 512 spectral scans.

* *Correspondence to: H. G. M. Edwards, Molecular Spectroscopy Group, Analytical Centre and Chemical and Forensic Sciences, School of Life Sciences, University of Bradford, Bradford, BD7 1DP, UK. E-mail: H.G.M.Edwards@bradford.ac.uk*

1 *Molecular Spectroscopy Group, Analytical Centre and Chemical and Forensic Sciences, School of Life Sciences, University of Bradford, Bradford, BD7 1DP, UK*

2 *Institute of Pharmaceutical Innovation, University of Bradford, Bradford, BD7 1DP, UK*

3 *Department of Pharmaceutical Analytical Chemistry, Faculty of Pharmacy, University of Assiut, Assiut, Egypt*

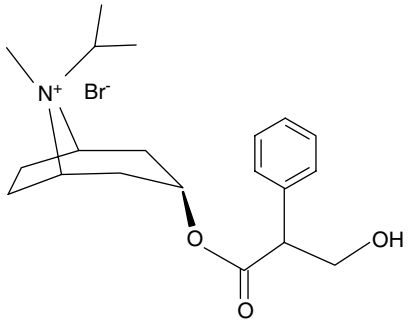

Scheme 1. The chemical structure of ipratropium bromide.

Calculation details

Calculations were performed on the IPRA cation (Fig. 1) using GAMESS-UK,[15] ORCA programmes[16] and BLYP density functional theory[17,18] with a 6-31G* basis set. Infrared and Raman spectra were calculated using the quasiharmonic approximation, through diagonalisation of the mass-weighted Hessian matrix. Intensities were calculated using the dipole-moment derivatives and the polarisability derivates of the normal modes. Two conformations of the IPRA cation were investigated. As can be seen in Fig. 1, the hydroxyl group is able to form an intramolecular hydrogen bond (conformer IPRA2). This conformation would be expected to be the most stable in the gas phase. In the solid state the hydroxyl group is able to form intramolecular hydrogen bonds and the conformation depicted in Fig. 1 (conformer IPRA1) may be important. Full geometry optimisation was carried out for both conformers, followed by a determination of the predicted vibrational frequencies.

Results and Discussion

Computational studies

Prior to the vibrational spectroscopic analysis, it is worth noting that the computed vibrational frequencies are sensitive to the theoretical method used and are generally shifted with respect to the experimental values. The predicted IR spectra of conformations IPRA1 and IPRA2 over the region 0–2000 cm^{-1} are compared in Fig. 2. The simulated spectra were generated by using the computed frequencies and intensities and applying a Gaussian broadening to each transition of 10 cm^{-1}. There is a clear shift in the C═O stretching at 1743 cm^{-1} (IPRA1) to 1718 cm^{-1} (IPRA2) resulting from the intramolecular hydrogen bonding. The strong absorption at 1134 cm^{-1} (IPRA1) shifts to 1110 cm^{-1} (IPRA2) corresponding to a coupled stretching of the C-O and C═O of the ester linkage.

The predicted Raman spectra of both IPRA1 and IPRA2 are dominated by the CH stretching bands. The region from 0–2000 cm^{-1} is shown in Fig. 3. The simulated spectra were generated by using the computed frequencies and intensities and applying a Gaussian broadening to each peak of 5 cm^{-1}. The most intense scattering, apart from the CH and OH region, is seen at 1595 cm^{-1} (IPRA1) and 1596 cm^{-1} (IPRA2). This is a stretching mode in the phenyl group. It is only seen with very weak intensity in the predicted IR spectra. The small shift in frequency between the two conformations reflects the small influence from the internal hydrogen bond on this vibrational mode.

The predicted Raman spectra are complex and are difficult to interpret in terms of conformational changes. The shifts in the predicted IR spectra of the two conformers are more straightforward to interpret and are summarised in comparison with the observed bands of IPRA in Table 1. It can be noted that the observed IR spectral features comprise the calculated IR spectral features of both IPRA1 and IPRA2. The very strong calculated bands at 1133 cm^{-1} and 1110 cm^{-1} of IPRA1 and IPRA2 respectively are recorded in the observed IR spectrum at 1225 and 1228 cm^{-1} and the strong calculated bands at 1743 and 1717 cm^{-1} of IPRA1 and IPRA2 respectively, are recorded in the observed IR spectrum at 1726 and 1712 cm^{-1}. These data suggest that the conformation in the solid state crystalline structure could be a mixture of IPRA1 and IPRA2.

Vibrational spectroscopic analysis

The infrared and Raman spectra of IPRA were recorded over the wavenumber range 4000–600 cm^{-1} and 4000–100 cm^{-1} respectively, using both transmission and attenuated total reflectance modes of operation in the former and 1064 nm excitation wavelength in the latter.

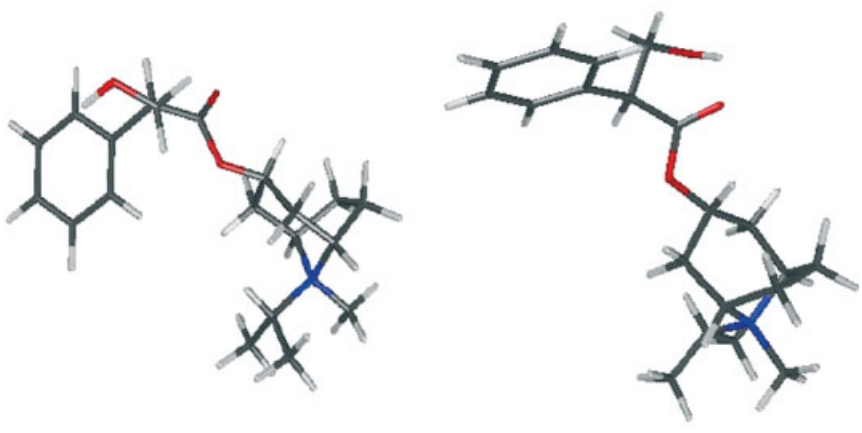

Figure 1. The calculated conformations of the IPRA cation; IPRA1 has no intramolecular hydrogen bond and IPRA2 with an intramolecular hydrogen bond.

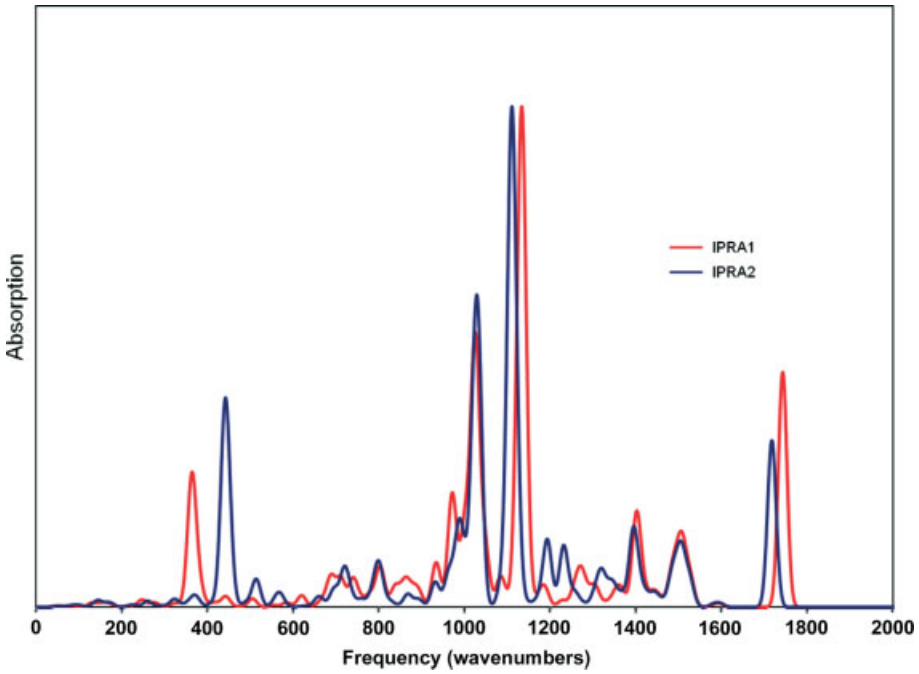

Figure 2. The calculated ipratropium cation IR conformational shifts in the region 0–2000 cm^{-1}.

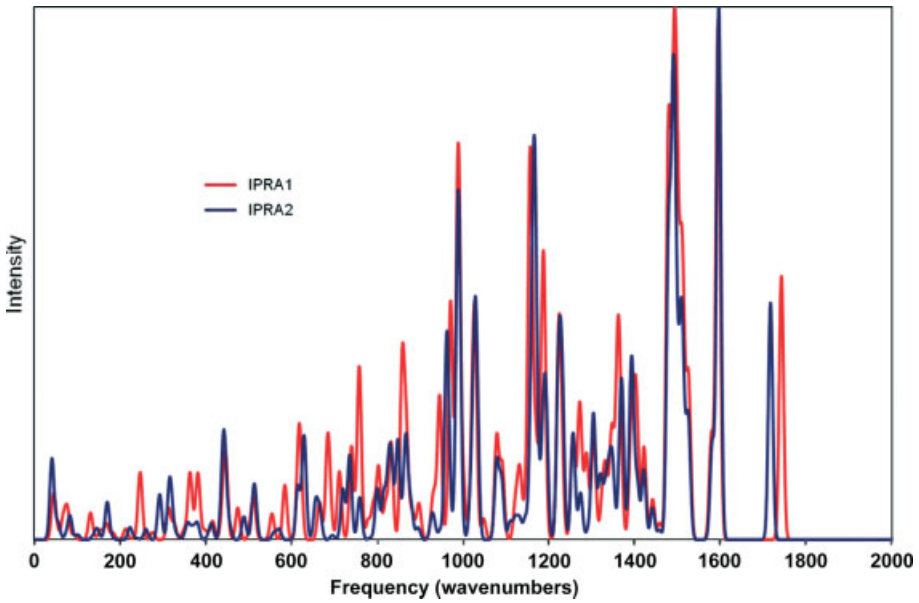

Figure 3. The calculated ipratropium cation Raman conformational shifts in the region 0–2000 cm^{-1}.

3800–2600 cm^{-1} region

The infrared and FT-Raman spectra are shown in Fig. 4; these spectra demonstrate clearly the complexity of the structural information that is obtained from the vibrational analysis; the OH stretching modes observed near 3500 cm^{-1} in the infrared spectrum are not observed in the Raman spectrum, whereas bands in the low wavenumber region that are normally characteristic of crystalline pharmaceutical forms are not recorded in the infrared spectrum. Experimental infrared and Raman wavenumbers are listed in Table 2 along with the calculated values; assignment of the major experimental vibrational features was carried out in the light of the computational results performed and the spectroscopic Raman data and the previously reported infrared data;[19] only very weak features in the observed spectra cannot be reliably assigned on the basis of the quantum chemical calculations.

The broad, rather diffuse υ(OH) stretching band (Fig. 4) in the infrared spectrum at 3492 cm^{-1} suggests that hydrogen bonding occurs in the crystalline IPRA. The CH stretching region comprises several features in the wavenumber range 3100–2800 cm^{-1} Fig. 4 for the infrared and Raman spectra; the CH stretching bands of the unsaturated, aromatic component of IPRA are more clearly shown in the Raman spectrum rather than in the infrared spectrum (Table 2) and can be assigned to the bands at 3067 and 3057 cm^{-1} in the Raman spectrum. The strong bands in the Raman spectrum

Table 1. The key calculated IR spectral features of IPRA1 and IPRA2 in comparison with the observed bands of IPRA in the range of 600–1800 cm^{-1}

Observed	IPRA1	Observed	IPRA2
700 m	698 w	667 w	669 w
741 m	745 mw		724 mw
804 w	800 mw	804 w	802 mw
852 w	849 w		874 w
868 vw	869 w	894 vw	891 vw
894 vw	891 w	934 w	936 mw
934 w	937 mw	989 vw	991 m
974 m	973 m	1029 w	1029 s
1029 w	1022 s	1228 s	1109 vs
1246 s	1134 vs	1327 w	1324 w
1273 w	1275 w	1348 w	1347 mw
1310 vw	1306 mw	1402 w	1397 m
1360 vw	1355 w	1452 ms	1450 w
1402 w	1403 m		1508 m
1452 ms	1450 w	1601 w	1595 w
	1508 m	1712 vs	1716 s
1601 w	1595 w		
1726 m,sh	1743 s		

at 2992 and 2968 cm^{-1} could be attributed to $\upsilon(CH_2\text{-}O\text{-})$ and $\upsilon_{as}(CH_2\text{-}OH)$ respectively.

1750–1550 cm^{-1} region

This is a very important spectroscopic region for structural studies – particularly for the C═O and C═C groups in this molecule. Expanded wavenumber regions of the infrared and Raman spectra are shown in Fig. 5. The observed infrared spectrum has a medium shoulder at 1726 cm^{-1} that can be assigned to υ(C═O), which is not involved in the hydrogen bonding, and a very strong band at 1712 cm^{-1} can be assigned to the carbonyl of the ester linkage upon the participation of the carbonyl group in the hydrogen bonding. These features suggest that IPRA specimen could be a mixture of the two conformations, IPRA1 and IPRA2.

The medium-intensity band at 1603 cm^{-1} in the Raman spectrum can be attributed to $\upsilon(CC)_{ring}$ quadrant vibration. There are several other features clearly seen in this wavenumber region at 1672, 1639, 1601, 1582 and 1712, 1649, 1583 cm^{-1} in the IR and Raman spectra, respectively; these features can be assigned on the basis of the quantum chemical calculations to molecular vibrations that involve both C═C and C═O groups and symmetric and asymmetric ring vibrations.

1800–100 cm^{-1} region

Infrared and Raman spectra over this wavenumber range are presented in Fig. 6; the infrared region comprises a rich spectrum from the C═O and C═C functionalities, which have already been discussed in some detail above, along with several bands of medium and strong intensities, whereas the Raman spectrum consists mainly of the strong C═C features and several other weaker features. In the range 1470–1300 cm^{-1}, we expect CH_3 and CH_2 aliphatic bending vibrations to occur with υ(CN) at around 1310 cm^{-1}.

Lower in wavenumber, there is more evidence that the IPRA sample could be a mixture of the two conformations IPRA1 and IPRA2, where the two strong bands in the calculated IR spectrum at 1134 and 1110 cm^{-1} (24 cm^{-1} shift) were observed in the experimental IR spectrum at 1246 and 1228 cm^{-1} (18 cm^{-1} shift), respectively. These two bands can be assigned on the basis of quantum chemical calculations as coupled stretching of the C-O and C═O of the ester linkage.

Then, in the 1050–850 cm^{-1} region we can expect modes arising from υ(C-OH) of the primary alcohols near 1040 cm^{-1} and OOC/CCH aromatic deformation modes. The υ(CNC) band is observed at around 850 cm^{-1}.

Finally, the complex ring modes of CCC deformations in the range between 690 and 500 cm^{-1} occur. The weak skeletal deformation bands are observed in the Raman spectrum below 440 cm^{-1} and the methyl torsional mode at 267 cm^{-1} of weak intensity can be noted.

A good overall agreement was obtained between the experimental and calculated frequency values (Table 2). However, even with the support of quantum chemical calculations, it is difficult to be certain about some of these molecular vibration assignments

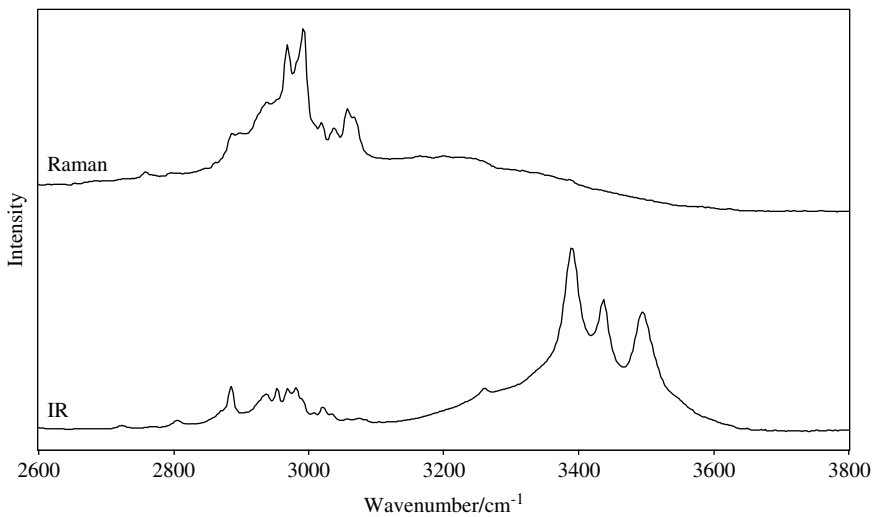

Figure 4. FT-Raman and IR spectral stackplot of IPRA in the 2600–3800 cm^{-1} region.

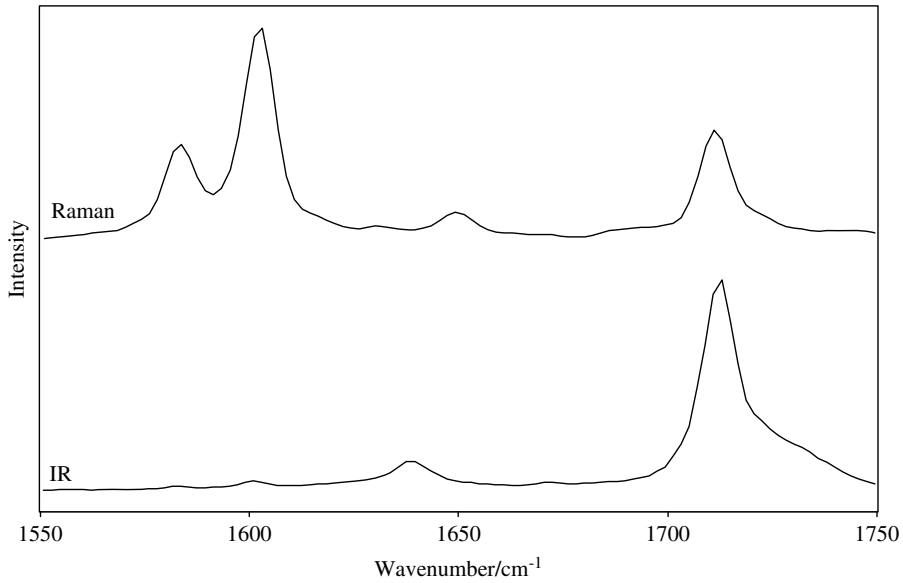

Figure 5. FT-Raman and IR spectral stackplot of IPRA in the 1550–1750 cm^{-1} region.

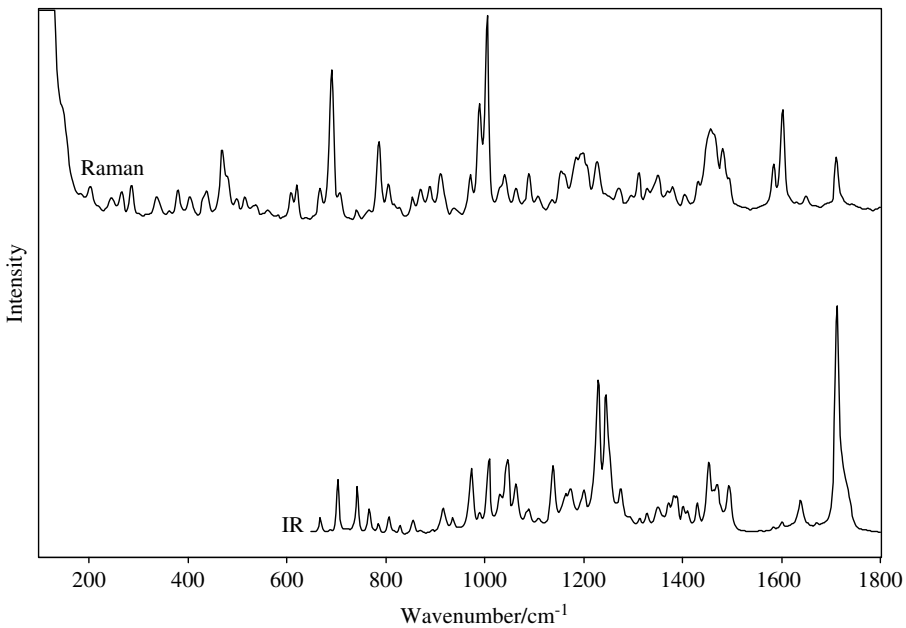

Figure 6. FT-Raman and IR spectral stackplot of IPRA in the 100–1800 cm^{-1} region.

in the mid-low wavenumber range because of the complexities of mode mixing; but it is clear that the major vibrational spectroscopic features of IPRA have been reasonably assigned in this study.

The key Raman spectral features observed for IPRA are the υ(CH) bands at 3057 and 3067 cm^{-1}, the $\upsilon(CH_2\text{-O-})$ band at 2992 cm^{-1}, the $\upsilon_{as}(CH_2\text{-OH})$ band at 2968 cm^{-1} the $\upsilon(CC)_{ring}$ band at 1603 cm^{-1}, the ring vibration band at 1006 cm^{-1}, the ring breathing band at 990 cm^{-1}, the out-of-plane $\delta(CH)_{ring}$ at 785 cm^{-1} and the out-of-plane δ (CCC) at 690 cm^{-1} while its key infrared spectral features are the υ(OH) band at 3492 cm^{-1}, the υ(C═O) band at 1712 cm^{-1}, the $\delta(CH)_{ring}$ and $\delta(CH_2)_{(sciss.)}$ band at 1492 cm^{-1}, the $\delta(CH_3)$ band at 1468 cm^{-1}, the ring stretch band at 1452 cm^{-1}, the coupled stretching of the C-O and C═O of the ester linkage bands at 1246 and 1228 cm^{-1}, the υ(C-OH) band at 1045 cm^{-1}, the ring vibration bands at 1006 and 741 cm^{-1}, the out-of-plane δ (CH) band at 970 cm^{-1} and the δ (COC) band at 700 cm^{-1}.

Conclusions

The Raman spectrum of ipratropium bromide was reported for the first time and quantum chemical calculations were successfully employed to analyse its structure, IR and Raman spectra. The differences in the vibrational modes of IPRA1 and IPRA2 were analysed, which provided insight into the structure of IPRA. In particular it was possible to indicate that IPRA specimens in the solid state could be a mixture of the two conformations IPRA1 and IPRA2 with and without intramolecular hydrogen bonding which would be useful for quality control of IPRA raw material and its

Table 2. The observed vibrational frequencies of IPRA and those calculated for IPRA cation. For calculated data, relative intensities for IPRA1 and IPRA2 were normalised such that the most intense band in the calculated spectra is 1

Observed		Calculated		
Raman, cm^{-1}	IR, cm^{-1}	IPRA1 υ (cm^{-1}) (Raman, IR Int.)	IPRA2 υ (cm^{-1}) (Raman, IR Int.)	Proposed assignment
	3492 ms	3552 (0.201,0.045)	3589 (0.230, 0.049)	υ(OH)
	3437 ms			
	3390 s			
	3258 w			
3067 m	3073 vw	3131 (1.000, 0.037)	3137 (1.000, 0.049)	Aromatic υ(CH)
3057 m	3057 vw	3059 (0.527, 0.023)	3058 (0.157, 0.002)	υ(CH)
3038 mw	3034 vw	3043 (0.169, 0.061)	3040 (0.322, 0.045)	$\upsilon_{as}(CH_2)$
3017 mw	3020 w	3026 (0.155, 0.020)	3025 (0.113, 0.013)	$\upsilon_{as}(CH_2)$
2992 s	3007 vw	3009 (0.141, 0.018)	3004 (0.756, 0.004)	$\upsilon(CH_2\text{-}O\text{-})$
	2979 w	3003 (0.014, 0.016)	2989 (0.067, 0.047)	$\upsilon_{as}(CH_2)$ & $\upsilon_{as}(CH_3)$
2968 s	2968 w	2933 (0.159, 0.164)	2969 (0.285, 0.059)	$\upsilon_{as}(CH_2\text{-}O\text{-}H)$
2952 w	2952 w			$\upsilon_{as}(CH_2)$
2938 w	2937 w			$\upsilon(CH_3)$
2896 vw				$\upsilon(CH_3)$
2886 w	2885 w			
	2871 sh,w			$\upsilon(CH_2)$
2861 w				
	2804 vw			
2757 w				
	2723 vw			
	1726 m,sh	1743 (0.061, 0.662)		υ(C═O)
1712 mw	1712 vs		1716 (0.081, 0.360)	υ(C═O)
	1672 vw			
1649 vw				$\upsilon(C{=}C)_{chain}$
	1639 mw			
1603 m	1601 w	1594 (0.120, 0.009)	1596 (0.183, 0.008)	$\upsilon(CC)_{ring}$
1583 w	1582 vw	1579 (0.024, 0.005)	1580 (0.033, 0.007)	
1493 sh,w	1492 m	1495 (0.006, 0.032)	1494 (0.049, 0.001)	$\delta(CH)_{ring}$ & $\delta(CH_2)_{(sciss.)}$
1481 mw		1482 (0.004, 0.071)	1482 (0.005, 0.048)	$\delta(CH_3)$
	1468 m	1478 (0.089, 0.005)	1478 (0.097, 0.004)	$\delta(CH_3)$
1456 br,m	1452 ms	1458 (0.004, 0.019)	1457 (0.003, 0.013)	Ring stretch
1431 w	1429 w	1421 (0.021, 0.035)	1421 (0.024, 0.026)	
1406 w	1408 w	1406 (0.015, 0.045)	1406 (0.018, 0.032)	In-plane $\delta(CH_3)$
	1402 w	1400 (0.026, 0.221)	1394 (0.038, 0.113)	δ (OH)& $\delta(CH_2)$
	1386 w	1391 (0.023, 0.013)	1390 (0.029, 0.048)	$\delta(CH_3)$ & $\delta(CH)_{chain}$
1380 w	1381 w			$\delta(CH_3)$
1370 sh,w	1372 w	1368 (0.013, 0.017)	1370 (0.029, 0.003)	
	1360 vw	1361 (0.035, 0.001)	1364 (0.011, 0.014)	
1348 w	1348 w	1355 (0.005, 0.028)	1348 (0.011, 0.009)	
1327 w	1327 w	1327 (0.006, 0.003)	1328 (0.007, 0.003)	δ (CH)
1312 w	1310 vw	1304 (0.025, 0.054)	1318 (0.018, 0.068)	υ(C-N) & $\delta(CH_3)$
1294 vw	1291 w,sh	1286 (0.016, 0.023)	1291 (0.003, 0.002)	δ (OH)& $\delta(CH_2)$
1271 w	1273 w	1273 (0.018, 0.036)	1273 (0.016, 0.008)	δ (CH-N)
	1246 s	1134 (0.004, 1.000)		Coupled stretching of the C-O and C═O of the ester linkage
1226 w	1228 s		1110 (0.006, 1.000)	Coupled stretching of the C-O and C═O of the ester linkage
1196 br,w	1199 w			
1185 w				
	1173 w			
1162 w	1161 w			
1155 w				
1137 vw	1137 m			
1110 vw	1105 vw			
1090 w	1088 w	1091 (0.017, 0.029)	1090 (0.018, 0.048)	
1063 w	1060 mw	1078 (0.022, 0.009)	1077 (0.024, 0.003)	

Table 2. (*Continued*)

Observed		Calculated		
Raman, cm^{-1}	IR, cm^{-1}	IPRA1 υ (cm^{-1}) (Raman, IR Int.)	IPRA2 υ (cm^{-1}) (Raman, IR Int.)	Proposed assignment
1040 w	1045 m	1047 (0.005, 0.161)	1032 (0.026, 0.323)	υ(C-OH)
	1029 w	1027 (0.036, 0.037)	1029 (0.031, 0.120)	υ(C-OH)
1006 ms	1006 m	1001 (0.011, 0.213)	1017 (0.008, 0.099)	Ring vibration
990 m	989 vw	988 (0.091, 0.017)	988 (0.106, 0.017)	Ring breathing
970 w	974 m	970 (0.053, 0.316)	968 (0.007, 0.011)	Out-of-plane δ (CH)
938 vw	934 w	933 (0.006, 0.113)	934 (0.001, 0.002)	
911 w	913 w	927 (0.005, 0.003)	926 (0.006, 0.002)	$\delta(CH_3)$
889 w	894 vw	897 (0.007, 0.007)	892 (0.001, 0.016)	OOC/CCH aromatic deformation
870 w	868 vw	867 (0.022, 0.033)	869 (0.002, 0.003)	
854 w	852 w	858 (0.040, 0.048)	847 (0.034, 0.002)	υ(C-N-C)
828 vw	826 w	831 (0.022, 0.002)	826 (0.021, 0.011)	Out-of-plane $\delta(CH)_{ring}$
816 vw		819 (0.008, 0.004)	815 (0.015, 0.003)	Skeletal vibrations
805 w	804 w	802 (0.017, 0.109)	799 (0.017, 0.091)	Skeletal vibrations
785 m	783 w	790 (0.008, 0.009)	784 (5.9e-4, 0.027)	Out-of-plane $\delta(CH)_{ring}$
764 vw	766 mw	757 (0.040, 0.019)	758 (0.014, 0.017)	Out-of-plane $\delta(CH)_{ring}$
742 vw	741 m	739 (0.022, 0.079)	735 (0.029, 0.020)	Ring vibration
708 w		711 (0.016, 0.079)	719 (0.017, 0.081)	Ring vibration
	700 m			δ (COC)
690 m	686 vw	690 (0.005, 0.051)	695 (0.002, 0.039)	Out-of-plane δ (CCC)
669 w	667 w	684 (0.022, 0.040)	665 (0.009, 0.012)	
639 vw		665 (0.009, 0.016)	656 (0.013, 0.012)	
621 w		621 (0.021, 0.023)	629 (0.036, 0.002)	Ring deformation
608 w		616 (0.018, 0.011)	614 (0.018, 0.001)	$\delta(CCC)_{ring}$
538 vw		554 (0.006, 0.006)	559 (0.002, 0.015)	δ (C-N)
515 vw		512 (0.009, 0.001)	514 (0.013, 0.044)	
499 vw		504 (0.003, 0.024)	510 (0.008, 0.018)	
479 sh,w		474 (0.007, 0.001)	489 (0.008, 0.009)	
470 mw		447 (0.010, 0.004)	455 (0.005, 0.031)	
438 w		439 (0.007, 0.019)	438 (0.014, 0.196)	In-plane $(CCC)_{ring}$ skeletal deformation
405 w		405 (0.001, 0.002)	405 (0.001, 2.3e-4)	In-plane (CCC) skeletal deformation
380 w		382 (0.015, 0.050)	380 ().005, 0.005)	δ (OH)
362 vw		360 (0.003, 0.011)	359 (0.005, 5.6e-4)	
337 w		326 (0.004, 0.010)	333 (0.001, 0.003)	Skeletal deformation
285 w		276 (0.002, 0.013)	292 (0.015, 0.004)	
267 w		249 (0.002, 0.003)	260 (0.004, 0.014)	$(CH_3)\tau$
240 w		247 (0.012, 0.017)	242 (1.1e-4, 4.3e-4)	

processed products. Quantum chemical calculations offer great potential to improve understanding of the structural properties of solid-state pharmaceuticals.

Acknowledgement

Hassan R. H. Ali is grateful for the support of the Government of the Arab Republic of Egypt during the period in which this work was carried out.

References

[1] S. C. Sweetman (Ed.). *Martindale, The Extra Pharmacopeia*, 34 edn, Pharmaceutical Press: London, **2005**.
[2] B. R. Buchanan, M. A. Baxter, T. S. Chen, X. Z. Qin, P. A. Robinson. *Pharm. Res.* **1996**, *13*, 616.
[3] A. Eustaquio, P. Graham, R. D. Jee, A. C. Moffat, A. D. Crafford. *Analyst* **1998**, *123*, 2303.
[4] M. Blanco, A. Eustaquio, J. M. Gonzalez, D. Serrano. *J. Pharm. Biomed. Anal.* **2000**, *22*, 139.
[5] T. Herkert, H. Prinz, K. A. Kovar. *J. Pharm. Biopharm.* **2001**, *51*, 9.
[6] W. Findlay, D. E. Bugay. *J. Pharm. Biomed. Anal.* **1998**, *16*, 921.
[7] J. Breitenbach, W. Schrof, J. Neumann. *Pharm. Res.* **1999**, *16*, 1109.
[8] L. S. Taylor, F. W. Langkilde. *J. Pharm. Sci.* **2000**, *89*, 1342.
[9] P. J. Hendra, H. M. M. Wilson, P. J. Wallen, I. J. Wesley, P. A. Bentley, M. Arruebarrena-Baez, J. A. Haigh, P. A. Evans, C. D. Dyer, R. Lehnert, M. V. Pellow-Jarman. *Analyst* **1995**, *120*, 985.
[10] C. Kontoyannis. *J. Pharm. Biomed. Anal.* **1995**, *13*, 73.
[11] C. Wang, J. Vickers, C. K. Mann. *J. Pharm. Biomed. Anal.* **1997**, *16*, 87.
[12] R. Neubert, B. Colin, S. Wartewig. *Pharm. Res.* **1997**, *14*, 946.
[13] L. S. Taylor, F. W. Langkilde. *Pharm. Res.* **1998**, *15*, 755.
[14] S. E. J. Bell, T. B. Burns, A. C. Dennis, J. S. Speers. *Analyst* **2000**, *125*, 541.
[15] M. F. Guest, I. J. Bush, H. J. J. Van Dam, P. Sherwood, J. M. H. Thomas, J. H. Van Lenthe, R. W. A. Havenith, J. Kendrick. *Mol. Phys.* **2005**, *103*, 719.
[16] F. Neese. *ORCA – An Ab Initio, Density Functional and Semiempirical Program Package, Version 2.4, Revision 45*, Max Planck Institut für Bioanorganische Chemie, Mülheim and der Ruhr, **2005**.

[17] A. D. Becke. *Physical Review A* **1988**, *38*, 3098.
[18] C. T. Lee, W. T. Yang, R. G. Parr. *Physical Review B* **1988**, *37*, 785.
[19] Electronic Handbook of FTIR Spectra, www.fdmspectra.com/fdm_ehb.htm, accessed 23 January **2009**.

